Physics of Fluids

Hydrodynamic force on a ship floating on the water surface near a semi-infinite ice sheet

Cite as: Phys. Fluids **33**, 127101 (2021); https://doi.org/10.1063/5.0071972
Submitted: 18 September 2021 • Accepted: 04 November 2021 • Published Online: 01 December 2021

Z. F. Li and G. X. Wu

Physics of Fluids ARTICLE scitation.org/journal/phf

Hydrodynamic force on a ship floating on the water surface near a semi-infinite ice sheet

Cite as: Phys. Fluids **33**, 127101 (2021); doi: 10.1063/5.0071972
Submitted: 18 September 2021 · Accepted: 4 November 2021 ·
Published Online: 1 December 2021

Z. F. Li[1] and G. X. Wu[2,a)]

AFFILIATIONS

[1]School of Naval Architecture and Ocean Engineering, Jiangsu University of Science and Technology, Zhenjiang 212003, China
[2]Department of Mechanical Engineering, University College London, Torrington Place, London WC1E 7JE, United Kingdom

[a)]Author to whom correspondence should be addressed: g.wu@ucl.ac.uk

ABSTRACT

The hydrodynamic problem of wave interaction with a ship floating on the water surface near a semi-infinite ice sheet is considered based on the linearized velocity potential theory for fluid flow and the thin elastic plate model for ice sheet deflection. The properties of an ice sheet are assumed to be uniform, and zero bending moment and shear force conditions are enforced at the ice edge. The Green function is first derived, which satisfies both boundary conditions on the ice sheet and free surface, as well as all other conditions apart from that on the ship surface. Through the Green function, the differential equation for the velocity potential is converted into a boundary integral equation over the ship surface only. An extended surface, which is the waterplane of the ship, is introduced into the integral equation to remove the effect of irregular wave frequencies. The asymptotic formula of the Green function is derived and its behaviors are discussed, through which an approximate and efficient solution procedure for the coupled ship/wave/ice sheet interactions is developed. Extensive numerical results through the added mass, damping coefficient and wave exciting force are provided for an icebreaker of modern design. It is found that the approximate method can provide accurate results even when the ship is near the ice edge, through which some insight into the complex ship/ice sheet interaction is investigated. Extensive results are provided for the ship at different positions, for different ice sheet thicknesses and incident wave angles, and their physical implications are discussed.

I. INTRODUCTION

Reduction of ice extent and thickness has led the Arctic to become a focal point for environmental protection and future developments. One of the new possible potentials is the new Arctic shipping route, which would substantially reduce the navigational distance between Asia, Europe, and North America, saving fuel and reducing CO_2 emissions. When sailing in the Arctic region, a ship may navigate in open water near the edge of a large ice sheet, instead of passing through icy water, to avoid the additional ice resistance and the possible damage to its structures. As a result, because of the effect of the nearby ice sheet, the hydrodynamic force on the ship as well as its performance will be very different from that in the open sea free of the ice sheet. This paper will undertake studies through a practical ship, and it aims to shed some insight into the behavior of the ship when navigating along the edge of a large ice sheet.

When an incident wave encounters a ship, it will be diffracted, and the wave will be altered. The ship will be set into motion, which creates more waves or wave radiation. In the completely open water, the diffracted and radiated waves will propagate into infinity. When there is an ice sheet near the ship, these waves will have further interactions with the ice sheet. Part of the wave will transmit into the region covered by the ice sheet. In addition to the wavy motion of the fluid, the ice sheet will also be set into motion in the form of a flexural-gravity wave, and the other part of the wave will be reflected back to the ship, together with the part of those due to ice sheet motion. This forward and backward interaction makes the hydrodynamic force on a ship near a large ice sheet much more complex than that in open waters, as well as its motion.

The wave motion without the presence of the ship is usually treated as the input of its environmental fluid loading. There has been extensive research on ocean wave interactions with large ice sheet, because in addition to the external loading to a ship it is of the strong interest in geophysics.[1] When the thickness of the ice sheet is much smaller than its horizontal dimension, the deflection of ice sheet can be modeled by the thin elastic plate. As water wave is very much dominated by gravity and viscosity effect becomes important only after many periods or many wavelengths, the fluid motion can be described through the velocity potential theory. When the wave amplitude is

small relative to this length, the conditions on the ice sheet and free surface can be linearized. This model has been widely used. Fox and Squire[2] solved two-dimensional (2D) problem-free surface wave interactions with a semi-infinite ice sheet through matched eigenfunction expansions (MEE), with the unknowns being found though minimizing the error function. The problem was extended to the oblique incident wave case by Fox and Squire,[3] and a critical angle was shown to exist when the wave number for free surface wave was larger than that for flexural-gravity wave in the ice sheet. When the angle between incident wave direction and ice edge was smaller than the critical angle, no wave energy could transmit into the far field below the ice sheet. Sahoo, Yip and Chwang[4] considered a similar problem with various edge conditions. In particular, instead of minimizing the error functions, they used an orthogonal inner product to enforce the edge conditions and continuity conditions at the interface of the free surface and ice sheet regions. The 2D problem was also solved by Balmforth and Craster[5] through the Wiener–Hopf method (WHM) with the ice sheet described by the Timoshenko–Mindlin model which further included the effects of rotary inertia and transverse shear of the ice sheet. For a typical range of ice properties and wave parameters, the dimensionless variables indicated that the Kirchhoff–Love model for thin elastic plate would give results similar to those by the Timoshenko–Mindlin model, which was consistent with the numerical results in Fox and Squire.[6] Based on the WHM, Tkacheva[7] derived the formula for the ice deflection, from which the far field reflection and transmission coefficients were obtained. Alternative to the MEE and WHM, Chakrabarti[8] solved the problem by first transforming it into a singular integral equation of the Carleman type over a semi-infinite range, and the solutions to the reflection and transmission coefficients were obtained. The residue calculus technique (RCT) was also used by Linton and Chung[9] to solve wave interactions with a semi-infinite ice sheet. Under the effect of wave propagations into the ice-covered water, the large ice sheet may break into discrete ice floes. This process was studied in a low temperature laboratory experiment by Dolatshah *et al.*[10] When the distance between two neighborhood ice sheets is much larger than the wavelength, the wide spacing approximation can be applied to construct an approximate solution, e.g., by Shi, Li, and Wu.[11]

When there is no ice sheet, various cases have been studied for a ship, e.g., floating in open water,[12] in a harbor,[13] and in a channel confined by two solid walls.[14] The interaction problem of coupled wave/body/ice sheet motions started only more recently. Sturova[15] derived a 2D Green function for the water surface covered by a semi-infinite ice sheet based on the MEE, and the wave radiation problem of a submerged oscillating cylinder was obtained through the boundary element method. The solution procedure was extended by Sturova[16] to the 2D ice channel confined by two semi-infinite ice sheets. The WHM can be also used to find the Green function for the water surface partially covered by an ice sheet, as done by Tkacheva[17] for a 2D ice floe. For a 2D rectangular barge floating on the channel confined between ice sheets, Ren, Wu and Thomas[18] obtained the solution through MEE and found that the hydrodynamic force oscillated against the wave number and multiple nature frequencies were found to be possible for the barge motions. Li, Shi and Wu[19] further developed a hybrid method for a 2D body of arbitrary shape, i.e., the boundary integral equation was used in the ice channel and the eigenfunction expansions were applied in the two ice-covered regions. When the distance between the ship and the edge of ice sheet is large, the effect of evanescent waves can be ignored in their interaction and only the progressing wave mode needs to be considered. Based on this, Li, Shi, and Wu[20] developed an approximate solution for a body floating on a wide polynya, and the mechanism for the oscillatory behaviors of the hydrodynamic forces was uncovered. When the submerged cylinder has a circular shape, the multipole expansion method (MEM) initiated in the free surface problem[21] can be used to the case for the water surface covered by an ice sheet, for example, by Tkacheva[22] for a cylinder near a vertical wall, by Li, Wu, and Ji[23] for a cylinder below an ice sheet with a crack and by Li, Shi, and Wu[24] for a cylinder undergoing large amplitude oscillations.

The three-dimensional (3D) problem has also been solved. Brocklehurst, Korobkin and Părău[25] analyzed flexural-gravity wave interactions with a bottom-mounted vertical circular cylinder clamped with the ice sheet through Weber transform and found that the horizontal force on the cylinder could be large even for small amplitude long waves. Similar problem was solved by Korobkin, Malenica, and Khabakhpasheva[26] through the vertical mode method (VMM). Ren, Wu, and Ji[27] extended the problem to multiple vertical circular cylinders through MEE, and the effects of arrangement of the cylinders on the hydrodynamic force were studied. In these works, the water surface is fully covered by an ice sheet. In many situations, there will be a region in which water surface may be free. Ren, Wu, and Ji[28] studied wave interactions with a vertical circular cylinder in a circular polynya, and the oscillatory features of the hydrodynamic force in the polynya were observed. For a practical structure floating in a polynya of arbitrary edge shape, Li, Shi, and Wu[29] developed a hybrid method in which a series of integral equations in horizontal plane under the ice sheet were constructed and coupled with the inner boundary integral equation through an orthogonal inner product. Similar solution procedure was used by Li, Shi, and Wu[30] for free surface wave interactions with an ice-covered harbor of vertical wall, and the shape of horizontal plane of which can be arbitrary. The solution procedure is efficient when the interface between two sub-domains is finite. For an ice channel with finite width and infinite length, Li, Wu and Ren[31] derived the Green function which satisfied all the boundary conditions except that on the body surface, based on which the problem of a ship in the channel was solved.

In this work, we shall further consider the problem of a ship navigating near the edge of a large ice sheet, in context of the possible Arctic shipping route. The large ice sheet is assumed to be semi-infinite extent with its edge being straight and infinitely long, and the water depth is assumed to be constant and finite. The differential equation for the disturbed velocity potential is first converted into a boundary integral equation based on the Green function, which satisfies all the boundary conditions apart from that on the ship surface. Through the asymptotic formula of the Green function, an approximate and efficient solution procedure is developed. Although the method is based on the assumption that a ship is far away from the ice sheet, it is found that the method can provide accurate results even when the ship is near the ice edge. Based on the asymptotic formula, the complex ship/wave/ice sheet interaction is investigated and the mechanism behind the behaviors of the hydrodynamic force is discussed.

The rest of paper is organized as follows. The mathematical model is formulated in Sec. II, and the governing equation together with the boundary conditions including those at the ice edge are

described. The Green function or the velocity potential due to a single oscillating source is given in Sec. III A, and the boundary integral equation for the radiation and diffraction potentials are presented in Sec. III B. Then the formula for the hydrodynamic force is provided in Sec. III C. Results and discussions are made in Sec. IV, where the asymptotic formula for the Green function is derived and an approximate solution procedure is developed. Finally, conclusions are drawn in Sec. V.

II. MATHEMATICAL MODEL

The hydrodynamic problem of wave interaction with a ship floating near a semi-infinite ice sheet is sketched in Fig. 1. The ice sheet is modeled as a thin elastic plate with uniform properties, i.e., its Young's modulus E, Poisson's ratio ν, density ρ_i and thickness h are assumed to be constant and its draught effect being ignored. To describe the problem, a Cartesian coordinate system $O-xyz$ is defined with $O-xy$ plane being the undisturbed mean free water surface, and z axis pointing vertically upward. The edge of the semi-infinite ice sheet is assumed to be straight and parallel to the x axis and located at $y=b$. The motion of the ship is assumed to be excited by an incident wave from the open water, which propagates from infinity from an angle β with the positive x axis. The fluid with density ρ_i is bounded in vertical direction by a flat seabed at $z=-H$ and an upper surface at $z=0$.

The fluid is assumed to be inviscid, incompressible, and homogeneous, and its motion to be irrotational. Thus, the velocity potential theory can be used to describe the fluid flow. When the amplitudes of wave motion and ship motion are small compared to wavelength and the dimension of ship, the linearized velocity potential theory can be further applied. For sinusoidal motion in time with radian frequency ω, the total velocity potential φ can be written as

$$\varphi(x,y,z,t)=\mathrm{Re}\left[\eta_0\phi_0(x,y,z)\mathrm{e}^{\mathrm{i}\omega t}+\sum_{j=1}^{6}\mathrm{i}\omega\eta_j\phi_j(x,y,z)\mathrm{e}^{\mathrm{i}\omega t}\right], \quad (1)$$

where η_0 is the amplitude of the incident wave, $\phi_0=\phi_I+\phi_D$ is the scattering potential with ϕ_I and ϕ_D as the incident and diffracted potentials, respectively; ϕ_j is the radiation potential due to the jth mode of ship motion in six degrees of freedom with complex amplitude η_j. Here, η_j with $j=1,\ 2,\ 3$ are for the translational modes along x, y and z directions, respectively, i.e., surge, sway and heave, while η_j with $j=4,\ 5,\ 6$ are for the corresponding rotational modes, i.e., roll, pitch and yaw. The conservation of mass requires that the velocity potential should satisfy the Laplace equation throughout the fluid, or

$$\nabla^2\phi_j+\frac{\partial^2\phi_j}{\partial z^2}=0\ (j=0,\ldots,6), \quad (2)$$

where $\nabla^2=\partial^2/\partial x^2+\partial^2/\partial y^2$ is the Laplacian in horizontal plane. In the fluid domain with a free surface, the combination of linearized dynamic and kinematic free surface boundary conditions provides

$$-\omega^2\phi_j+g\frac{\partial\phi_j}{\partial z}=0\ \ (y\le b-0\ \text{and}\ z=0), \quad (3)$$

where g is the acceleration due to gravity. In the fluid domain covered by an ice sheet, it is assumed that there is no gap between ice sheet and water surface, which provides the following kinematic condition:

$$\frac{\partial W}{\partial t}=\frac{\partial\Phi}{\partial z}\ (y\ge b+0\ \text{and}\ z=0). \quad (4)$$

Here, W is the deflection of the ice sheet, which may be written in an analogous form to Eq. (1), or

$$W(x,y,t)=\mathrm{Re}\left[\eta_0 w_0(x,y)\mathrm{e}^{\mathrm{i}\omega t}+\sum_{j=1}^{6}\mathrm{i}\omega\eta_j w_j(x,y)\mathrm{e}^{\mathrm{i}\omega t}\right]. \quad (5)$$

This combined with Eq. (4) means that

$$w_j=\frac{1}{\mathrm{i}\omega}\frac{\partial\phi_j}{\partial z}\bigg|_{z=0}. \quad (6)$$

The combination of the kinematic and dynamic boundary conditions on the interface between ice sheet and water surface provides

$$(L\nabla^4+\rho_w g-m_i\omega^2)\frac{\partial\phi_j}{\partial z}-\rho_w\omega^2\phi_j=0\ (y\ge b+0\ \text{and}\ z=0), \quad (7)$$

where $L=Eh^3/[12(1-\nu^2)]$ is the effective flexural rigidity of the ice sheet, and $m_i=\rho_i h$ is the corresponding mass per unit area. Here,

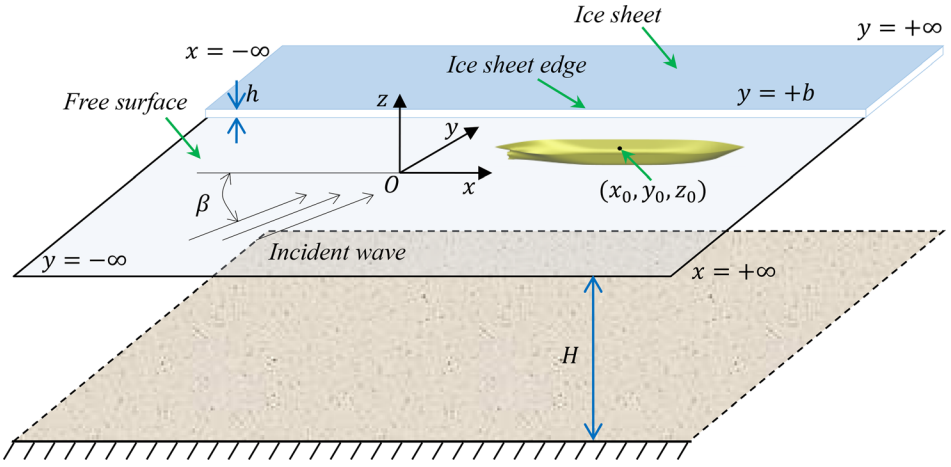

FIG. 1. Coordinate system and sketch of the problem.

$b-0$ and $b+0$ in Eqs. (3) and (7) indicate that the ice edge is approached from the free surface side and ice sheet side, respectively. At the ice edge, zero bending moment and shear force conditions are imposed, which can be written as[32]

$$\mathcal{B}\left(\frac{\partial\phi_j}{\partial z}\right)=0 \text{ and } \mathcal{S}\left(\frac{\partial\phi_j}{\partial z}\right)=0 \ (y=b+0 \text{ and } z=0) \quad (8)$$

for $j=0,\ldots,6$, with the operators $\mathcal{B}$ and $\mathcal{S}$, respectively, defined as

$$\mathcal{B}=\frac{\partial^2}{\partial y^2}+\nu\frac{\partial^2}{\partial x^2}, \quad (9)$$

$$\mathcal{S}=\frac{\partial}{\partial y}\left[\frac{\partial^2}{\partial y^2}+(2-\nu)\frac{\partial^2}{\partial x^2}\right]. \quad (10)$$

On the mean wetted ship surface S_B, the impermeable condition provides

$$\frac{\partial\phi_j}{\partial n}=n_j \quad \text{and} \quad \frac{\partial\phi_D}{\partial n}=-\frac{\partial\phi_I}{\partial n} \ (j=1,\ldots,6), \quad (11)$$

where $(n_1,n_2,n_3)=\vec{n}$, $(n_4,n_5,n_6)=(\vec{r}-\vec{r}_0)\times\vec{n}$, with $\vec{n}$ being the unit normal vector of the surface pointing into the ship, $\vec{r}=(x,y,z)$ being the position vector and $\vec{r}_0=(x_0,y_0,z_0)$ being the rotational center. Similarly, on the flat seabed $z=-H$, we have

$$\frac{\partial\phi_j}{\partial z}=0 \quad \text{and} \quad \frac{\partial\phi_D}{\partial z}=0 \ (j=1,\ldots,6) \quad (12)$$

for $j=0,\ldots,6$. At infinity, the radiation condition requires that the radiated and diffracted waves should propagate outward in form of free surface wave for $y\le b-0$ and in form of flexural-gravity wave for $y\ge b+0$.

III. SOLUTION PROCEDURE

A. Velocity potential due to a single source: The Green function

The Green function $G(p,q)$ is defined as the velocity potential at field point $p(x,y,z)$ due to a source at point $q(\xi,\eta,\zeta)$. Once G is obtained, the unknown velocity potential described in Sec. II can be found through the boundary integral equation. G should satisfy the following governing equation throughout the fluid or

$$\nabla^2 G+\frac{\partial^2 G}{\partial z^2}=-4\pi\delta(x-\xi)\delta(y-\eta)\delta(z-\zeta) \quad (13)$$

together with the boundary conditions in (3), (7), (8), (12) and the radiation condition. Here, $\delta(x)$ is the Dirac delta function. Without loss of generality, we may assume that the source is in the free surface part or $\eta\le b-0$, which is consistent with the location of the ship floating on the free surface. Then following the similar procedure in Li, Wu, and Ren,[31] we can first apply the Fourier transform along the x axis. In the z direction, vertical modes $Z_m(z)$ $(m=0,1,\ldots,\infty)$ below the free surface $y\le b-0$ and $Q_m(z)$ $(m=-2,-1,\ldots,\infty)$ below the ice sheet $y\ge b+0$ can be used, and they are written as[29]

$$Z_m(z)=\frac{\cosh[k_m(z+H)]}{\cosh(k_mH)}, \quad (14)$$

$$Q_m(z)=\frac{\cosh[\kappa_m(z+H)]}{\cosh(\kappa_mH)}, \quad (15)$$

where k_m are the root of the dispersion equation for free surface (k_0 is the purely positive real root; k_m are an infinite number of purely negative imaginary roots with $m=1,\ldots,\infty$) or

$$K_1(\omega,k)=gk\tanh(kH)-\omega^2=0 \quad (16)$$

and κ_m being the root of the dispersion equation for ice sheet (κ_{-2} and κ_{-1} are two complex roots with negative imaginary parts and symmetric about the imaginary axis; κ_0 is the purely positive real root; κ_m are an infinite number of purely negative imaginary roots with $m=1,\ldots,\infty$) or

$$K_2(\omega,k)=(Lk^4+\rho_w g-m_i\omega^2)k\tanh(kH)-\rho_w\omega^2=0. \quad (17)$$

Equation (13) then becomes a series of standard second order ordinary different equations in the y direction, which can be easily solved, similar to that in Li, Wu, and Ren.[31] Here, we write the result as

$$G=\begin{cases} F+2\sum_{m=0}^{\infty}Z_m(z)\int_0^{+\infty}a_m e^{-i\beta_m(b-y)}\cos[\alpha(x-\xi)]d\alpha, & y\le b-0,\\ 2\sum_{m=-2}^{\infty}Q_m(z)\int_0^{+\infty}b_m e^{-i\gamma_m(y-b)}\cos[\alpha(x-\xi)]d\alpha, & y\ge b+0, \end{cases} \quad (18)$$

where $\beta_m^2=k_m^2-\alpha^2$ and $\gamma_m^2=\kappa_m^2-\alpha^2$. To satisfy the condition in the far field, we choose $\mathrm{Im}(\beta_m)\le 0$ and $\mathrm{Im}(\gamma_m)\le 0$ when they are a complex number, and $\beta_m>0$ and $\gamma_m>0$ when they are a purely real number. In Eq. (18),

$$F=\sum_{m=0}^{\infty}\frac{\pi}{iP_m}Z_m(\zeta)Z_m(z)H_0^{(2)}(k_mR) \quad (19)$$

is in fact the Green function for full free surface without the ice sheet, where $H_0^{(2)}(k_mR)$ is the zeroth order Hankel function of the second kind. Equation (19) can be also written in an integral form as[33]

$$F=\frac{1}{r_1}+\frac{1}{r_2}+2\int_0^{+\infty}e^{-kH}\frac{gk+\omega^2}{K_1(\omega,k)}\frac{\cosh[k(\zeta+H)]}{\cosh(kH)}\times\cosh[k(z+H)]J_0(kR)dk, \quad (20)$$

where the integral route from 0 to $+\infty$ should pass over the pole at $k=k_0$, r_1 is the distance between p and q, r_2 is the distance between p and the mirror image of q about the flat seabed, $J_0(kR)$ is the zeroth order Bessel function of the first kind, and R is the horizontal distance between p and q. The unknown coefficients a_m and b_m in Eq. (18) can be obtained through enforcing the continuity at the interface at $y=b$ and the ice edge conditions along $y=b$, $z=0$, or the solution of the following matrix equation:[31]

$$\gamma_m\sum_{\tilde{m}=0}^{\infty}a_{\tilde{m}}V_{m,\tilde{m}}-b_m\gamma_mU_m-\frac{LT_m}{\rho_w\omega^2}\sum_{\tilde{m}=-2}^{\infty}b_{\tilde{m}}T_{\tilde{m}}\left[\nu\alpha^2(\gamma_{\tilde{m}}+\gamma_m)-2\alpha^2\gamma_m+\gamma_m^2(\gamma_{\tilde{m}}-\gamma_m)-\gamma_{\tilde{m}}(\kappa_m^2+\kappa_{\tilde{m}}^2)\right]=i\gamma_m\sum_{\tilde{m}=0}^{\infty}\frac{1}{\beta_{\tilde{m}}P_{\tilde{m}}}e^{-i\beta_{\tilde{m}}(b-\eta)}Z_{\tilde{m}}(\zeta)V_{m,\tilde{m}} \quad (21)$$

and

$$-\beta_m P_m a_m - \sum_{\tilde{m}=-2}^{\infty} b_{\tilde{m}} \gamma_{\tilde{m}} V_{\tilde{m},m} = \mathrm{i} e^{-\mathrm{i}\beta_m(b-\eta)} Z_m(\zeta), \tag{22}$$

where

$$T_m = \kappa_m \tanh(\kappa_m H), \tag{23}$$

$$U_m = \frac{2\kappa_m H + \sinh(2\kappa_m H)}{4\kappa_m \cosh^2(\kappa_m H)} + \frac{2LT_m^2\kappa_m^2}{\rho_w \omega^2}, \tag{24}$$

$$V_{m,\tilde{m}} = \int_{-H}^{0} Q_m Z_{\tilde{m}} \mathrm{d}z = \frac{T_m - \omega^2/g}{\kappa_m^2 - k_{\tilde{m}}^2}, \tag{25}$$

$$P_m = \int_{-H}^{0} Z_m(z) Z_m(z) \mathrm{d}z = \frac{2k_m H + \sinh(2k_m H)}{4k_m \cosh^2(k_m H)}. \tag{26}$$

It should be noticed that the Green function in Eq. (18) satisfies all the boundary conditions apart from that on the mean wetted body surface.

B. Boundary integral equation for the disturbed velocity potential

As demonstrated by Li, Wu, and Ren,[31] with the help of the Green function G in (18), we can write the disturbed velocity potential ϕ in terms of a boundary integral equation over the mean wetted ship surface only, or

$$\ell\phi(p) = \int_{S_B} \left[G(p,q) \frac{\partial \phi(q)}{\partial n_q} - \frac{\partial G(p,q)}{\partial n_q} \phi(q) \right] \mathrm{d}s_q, \tag{27}$$

where ℓ is the solid angle at point p. For a given condition in Eq. (11), Eq. (27) may be solved. However, at some frequencies, solution of Eq. (27) may not exist or may not be unique. This has been widely discussed in the free surface problem and is commonly called irregular frequencies. These frequencies may be linked to the velocity potential flow problem inside the space confined by the ship hull. The internal potential is zero on the inner hull surface and satisfies the same condition as that of G on the waterplane of the ship. In general, the solution of the potential will be zero. However, at irregular frequencies, non-trivial solution may exist. Since G in Eq. (18) satisfies Eq. (3), with or without the ice sheet, the irregular frequencies here are expected to be the same as those for the free surface problem. It ought to point out that the existence of the irregular frequencies is a result of the integral equation in Eq. (27) and it is not a real physical problem. Therefore, their effects can be removed through modifying Eq. (27). Here, we adopt the procedure in Lee, Newman, and Zhu[34] and rewrite Eq. (27) in an equivalent form as

$$\ell\phi(p) + \int_{S_B+S_E} \frac{\partial G(p,q)}{\partial n_q} \phi(q) \mathrm{d}s_q = \int_{S_B} G(p,q) \frac{\partial \phi(q)}{\partial n_q} \mathrm{d}s_q \quad \text{for } p \in S_B \tag{28}$$

and

$$-4\pi\phi(p) + \int_{S_B+S_E} \frac{\partial G(p,q)}{\partial n_q} \phi(q) \mathrm{d}s_q = \int_{S_B} G(p,q) \frac{\partial \phi(q)}{\partial n_q} \mathrm{d}s_q \quad \text{for } p \in S_E, \tag{29}$$

where S_E is the extended surface interior the ship or its waterplane at $z = 0$.

For the radiation potential $\phi = \phi_j$, the boundary integral equations (28) and (29) can be solved directly by imposing $\partial\phi_j/\partial n = n_j$ on S_B. While the diffracted velocity potential ϕ_D of the incident velocity potential ϕ_I includes two components, i.e.,

$$\phi_D = \phi_D^{(1)} + \phi_D^{(2)}, \tag{30}$$

where $\phi_D^{(1)}$ is the diffracted velocity potential by the ice sheet to ϕ_I, and $\phi_D^{(2)}$ is that by the body to $\varphi = \phi_I + \phi_D^{(1)}$. The incident velocity potential for free surface wave can be written as

$$\phi_I = \varphi_I(y,z) \mathrm{e}^{-\mathrm{i}k_x x}, \tag{31}$$

with

$$\varphi_I(y,z) = A \mathrm{e}^{-\mathrm{i}k_y y} Z_0(z), \tag{32}$$

where $A = \mathrm{i}g/\omega$, $k_x = k_0 \cos\beta$ and $k_y = k_0 \sin\beta$. Correspondingly, the velocity potential φ can be written as

$$\varphi = \bar{\varphi}(y,z) \mathrm{e}^{-\mathrm{i}k_x x}. \tag{33}$$

Then, φ can be obtained virtually in the same way as that used for $\tilde{G}$, through replacing α in Eqs. (21) and (22) with k_x, and the right hand sides of the matrix equation with the contribution due to ϕ_I, as shown in the Appendix. Through the decomposition (30), both φ and $\phi_D^{(2)}$ satisfy the free ice edge conditions (8), and the latter one can be solved through the boundary integral equations (28) and (29) by imposing the condition $\partial\phi_D^{(2)}/\partial n = -\partial\varphi/\partial n$ on the mean wetted ship surface S_B.

C. Hydrodynamic coefficients and wave exciting force

After the velocity potential ϕ_j have been found, the pressure at any point in fluid can be computed through the linearized Bernoulli equation. Then the hydrodynamic force on a ship can be obtained through integrating the dynamic pressure over the mean wetted ship surface. According to the decomposition of velocity potential in Eq. (1), we may divide the total hydrodynamic force into two parts, i.e., the wave exciting force $f_{E,j}$ at unit incident wave amplitude due to the scattering velocity potential ϕ_0 or

$$f_{E,j} = -\mathrm{i}\omega\rho_w \int_{S_B} \phi_0 n_j \mathrm{d}s \tag{34}$$

and the radiation force due to the forced oscillatory motions of a ship which can be written in form of added mass μ_{jk} and damping coefficient λ_{jk}, i.e.,

$$\tau_{jk} = \mu_{jk} - \mathrm{i}\frac{\lambda_{jk}}{\omega} = \rho_w \int_{S_B} \phi_k n_j \mathrm{d}s. \tag{35}$$

IV. NUMERICAL RESULTS

In following numerical computations, the values of parameters of ice sheet and fluid are taken to be[35]

$$E = 5\,\mathrm{GPa}, \quad \nu = 0.3, \quad \rho_i = 922.5\,\mathrm{kg/m^3}, \quad \rho_w = 1025\,\mathrm{kg/m^3}, \quad H = 100\,\mathrm{m}, \tag{36}$$

together with $h \in [0\,\mathrm{m},\ 5\,\mathrm{m}]$, which are one of the typical situations in the Arctic region. When there is no special specification with unit of

the parameter being given, the numerical results are dimensionalized based on the combinations of three basic parameters, i.e., density of water ρ_w, acceleration due to gravity $g = 9.80\,\mathrm{m/s^2}$ and the half breadth of the ship. The infinite summations in Eq. (18) are truncated at a finite number M_G. Similarly, only the first M_D terms are kept in the infinite summations in Eqs. (A2) and (A4). For the boundary integral equations (28) and (29), the mean wetted body surface S_B is discretized into N_B flat panels and the extended interior surface S_E introduced to remove the irregular frequencies is discretized into N_E flat panels. On each panel, the velocity potential is assumed to be constant. The application of flat panels indicates that the solid angle ℓ in Eq. (28) is always 2π. Through increasing M_G, M_D, N_B and N_E, a desired accuracy can be obtained. The solution procedure developed in Sec. III can be used to compute all the hydrodynamic coefficients and wave exciting force, and only the heave and roll modes are provided in the following text to show the effect of ice sheet.

A. Geometry and principal parameters of the ship

The ship used for this study is an icebreaker of modern design. The principal parameters are given in Table I, in which the vertical position of gravity center is given with respect to the baseline, the longitudinal position is with respect to the after-perpendicular, and the transverse position is with respect to the longitudinal middle plane. The rotational center (x_0, y_0, z_0) of the ship is taken to be at the gravitational center, and $y_0 = 0$ has been used below. A typical discretization of the hull surface for the boundary integral equations (28) and (29) are shown in Fig. 2. On the mean wetted body surface S_B, $N_B = 2870$ flat panels are distributed, and the extended interior surface S_E is discretized into $N_E = 172$ flat panels. Near the bow and stern, the triangle element is used. Away from these areas, where the surface is less curved, the quadrilateral element is used, starting with smaller one and followed by larger one toward the middle section. It may be noticed that the mesh quality and quantity will have an influence on the computed results, and a proper mesh can reduce the number of panels to meet the requirement of convergence. For the infinite summation in Eq. (18), $M_G = 50$ is taken. To obtain the diffracted velocity potential $\phi_D^{(1)}$ due to ϕ_I by the semi-infinite ice sheet, $M_D = 200$ is taken. It has been observed that further increase in N_B, N_E, M_G and M_D will no longer give graphically distinguishable curves in the figures. They are used for the results below if it is not specified.

TABLE I. The principal parameters of a modern design icebreaker.

Length between perpendiculars (L)	147.20 m
Breadth (B)	22.60 m
Draft (T)	8.00 m
Displacement volume (D)	17 543.10 $\mathrm{m^3}$
Block coefficient (C_b)	0.66
Mid-ship coefficient (C_m)	0.93
Vertical center of gravity	10.00 m
Longitudinal center of gravity	70.27 m
Transverse center of gravity	0.00 m
Roll gyration radius	0.34B
Pitch gyration radius	0.27L
Yaw gyration radius	0.27L

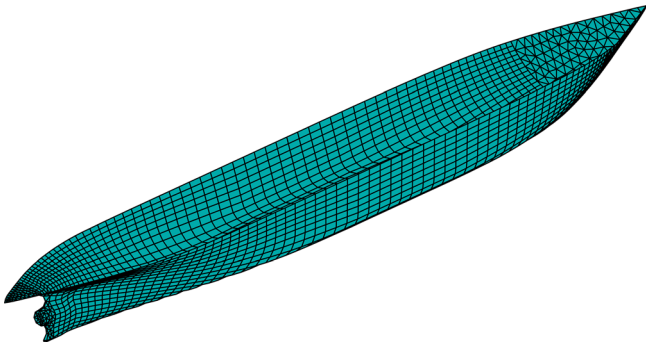

FIG. 2. General view of the geometry and distribution of panels on the icebreaker.

B. Asymptotic wave behaviors at large b through the Green function

For waves generated by an oscillating source submerged in a channel confined between two semi-infinite ice sheets, it has been shown that when $\kappa_0 < k_0$, there may be waves trapped in the channel with N discrete wavenumbers at $\kappa_0 < \alpha_j < k_0$, $j = 1, \ldots, N$, and the value of N will depend on a particular problem.[36] These waves propagate periodically along the channel and decay exponentially away from the channel in its transverse direction. α_j corresponds to the first order singular points of integrand of Green function.[31] For the current problem, i.e., when there is a semi-infinite ice sheet on one side, no such simple poles are found numerically for a_m and b_m in Eq. (18). This means that the free surface waves of the form $\exp[-\mathrm{i}\beta_{0,j}(b-y)]\exp(-\mathrm{i}\alpha_j|x-\xi|)$ with $\beta_{0,j} = \sqrt{k_0^2 - \alpha_j^2}$, which does not decay at large x or large b, will not appear.

To consider the asymptotical behavior at large b, Eqs. (21) and (22) may be rewritten as

$$a_m = -\frac{1}{\beta_m P_m}\left[\mathrm{i}e^{-\mathrm{i}\beta_m(b-\eta)}Z_m(\zeta) + \sum_{\tilde{m}=-2}^{\infty} b_{\tilde{m}}\gamma_{\tilde{m}}V_{\tilde{m},m}\right] \tag{37}$$

and

$$\begin{aligned}-\gamma_m\sum_{n=-2}^{\infty} b_n\gamma_n\sum_{\tilde{m}=0}^{\infty}\frac{1}{\beta_{\tilde{m}}P_{\tilde{m}}}V_{n,\tilde{m}}V_{m,\tilde{m}} - b_m\gamma_m U_m - \frac{LT_m}{\rho_w\omega^2}\sum_{\tilde{m}=-2}^{\infty} b_{\tilde{m}}T_{\tilde{m}}\\ \times\left[(\nu-2)\alpha^2(\gamma_{\tilde{m}}+\gamma_m) - \gamma_m^3 - \gamma_{\tilde{m}}^3\right]\\ = 2\mathrm{i}\gamma_m\sum_{\tilde{m}=0}^{\infty}\frac{1}{\beta_{\tilde{m}}P_{\tilde{m}}}e^{-\mathrm{i}\beta_{\tilde{m}}(b-\eta)}Z_{\tilde{m}}(\zeta)V_{m,\tilde{m}}.\end{aligned} \tag{38}$$

When $m > 0$, β_m is a negative imaginary number and $\exp[-\mathrm{i}\beta_m(b-y)]$ as well as $\exp[-\mathrm{i}\beta_m(b-\eta)]$ decay exponentially with b. Therefore, we need to consider only the term of a_0 and keep only the term of $\tilde{m} = 0$ on the right hand side of Eq. (38). As $\beta_0^2 = k_0^2 - \alpha^2 \to 0$ when $\alpha \to k_0$, there is a square root singularity in a_0 of form $1/\beta_0$. If we multiply β_0 on both sides of Eq. (38), we can see that b_m has no singularity at $\beta_0 = 0$. From Eq. (37), a_0 can then be written as

$$a_0 = A(\alpha)e^{-\mathrm{i}\beta_0(b-\eta)}Z_0(\zeta)/\beta_0, \tag{39}$$

where $A(\alpha)$ has no singularity. Equation (39) can be further written as

$$a_0 = a_0^{(1)} + a_0^{(2)}, \tag{40}$$

where

$$a_0^{(1)} = [A(\alpha) - A(k_0)]e^{-i\beta_0(b-\eta)}Z_0(\zeta)/\beta_0, \tag{41}$$

$$a_0^{(2)} = A(k_0)e^{-i\beta_0(b-\eta)}Z_0(\zeta)/\beta_0. \tag{42}$$

The second term on the right hand side of Eq. (18) for $y \le b - 0$ can be written as

$$G_I = \sum_{m=0}^{\infty} g_m, \tag{43}$$

where

$$g_m = 2Z_m(z)\int_0^{+\infty} a_m e^{-i\beta_m(b-y)}\cos[\alpha(x-\xi)]d\alpha \ (m = 0, \ldots, \infty). \tag{44}$$

At large b, we can keep only g_0 term. We write

$$g_0 = g_0^{(1)} + g_0^{(2)}, \tag{45}$$

where

$$g_0^{(1)} = 2Z_0(z)\int_0^{+\infty} a_0^{(1)}e^{-i\beta_0(b-y)}\cos[\alpha(x-\xi)]d\alpha, \tag{46}$$

$$g_0^{(2)} = 2Z_0(z)\int_0^{+\infty} a_0^{(2)}e^{-i\beta_0(b-y)}\cos[\alpha(x-\xi)]d\alpha. \tag{47}$$

Invoking Eq. (A6) of Li, Wu, and Ren,[31] we may rewrite Eq. (47) as

$$g_0^{(2)} = \pi A(k_0)Z_0(z)Z_0(\zeta)H_0^{(2)}(k_0\bar{R}), \tag{48}$$

where $\bar{R}^2 = (x-\xi)^2 + (2b-y-\eta)^2$. By noticing[37]

$$H_0^{(2)}(\bar{R}) = \sqrt{\frac{2}{\pi\bar{R}}}e^{-i\left(\bar{R}-\frac{\pi}{4}\right)} + O\left(\frac{1}{\bar{R}^{3/2}}\right) \quad \text{for } \bar{R} \to +\infty, \tag{49}$$

we further have

$$\lim_{\bar{R}\to+\infty} g_0^{(2)} = A(k_0)Z_0(z)Z_0(\zeta)\sqrt{\frac{2\pi}{k_0\bar{R}}}e^{-i\left(k_0\bar{R}-\frac{\pi}{4}\right)}. \tag{50}$$

For $g_0^{(1)}$ in Eq. (46), let $i(x-\xi) = \bar{R}\sinh t'$ and $2b-y-\eta = \bar{R}\cosh t'$ with $t' \in (-i\pi/2, +i\pi/2)$, and $\alpha = ik_0\sinh t$ and $\beta_0 = k_0\cosh t$, we have

$$g_0^{(1)} = iZ_0(z)Z_0(\zeta)\int_C [A(\alpha) - A(k_0)]e^{-ik_0\bar{R}\cosh(t-t')}dt, \tag{51}$$

where C is the integral route below,

$$t \in (-\infty + i\pi/2, +i\pi/2) \cup (+i\pi/2, -i\pi/2) \cup (-i\pi/2, -i\pi/2+\infty). \tag{52}$$

By using the method of steepest descent, we have the asymptotic formula of Eq. (51),

$$\lim_{\bar{R}\to+\infty} g_0^{(1)} = Z_0(z)Z_0(\zeta)[A(\alpha_0) - A(k_0)]\sqrt{\frac{2\pi}{k_0\bar{R}}}e^{-i\left(k_0\bar{R}-\frac{\pi}{4}\right)}, \tag{53}$$

where

$$\alpha_0 = -k_0\sin(\theta_0), \tag{54}$$

with

$$\theta_0 = \arctan[(x-\xi)/(2b-y-\eta)]. \tag{55}$$

Invoking Eqs. (50) and (53), we can obtain the asymptotic expression of Eq. (43) as

$$G_I^{\infty} \equiv \lim_{\bar{R}\to+\infty} G_I = A(\alpha_0)Z_0(z)Z_0(\zeta)\sqrt{\frac{2\pi}{k_0\bar{R}}}e^{-i\left(k_0\bar{R}-\frac{\pi}{4}\right)}, \tag{56}$$

where the higher order term has been dropped. It may be noticed that $A(\alpha)$ in Eq. (56) in the above equation can be obtained numerically through the matrix equation (37) and (38). As $b \to +\infty$, $\theta \to 0$ and $\alpha_0 \to 0$, we further have

$$\lim_{b\to+\infty} G_I^{\infty} = A(0)Z_0(z)Z_0(\zeta)\sqrt{\frac{2\pi}{k_0\bar{b}}}e^{-i\left(k_0\bar{b}-\frac{\pi}{4}\right)}, \tag{57}$$

where $\bar{b} = 2b - y - \eta$. Equation (57) shows that at large b, the effect of the ice sheet on the free surface decays at a rate of $1/\mathrm{sqrt}(\bar{b})$. It is in fact due to a source placed at mirror image position of q with respect to $y = b$. However, it does not mean $y = b$ can be treated as a wall, as the strength of the source is different, and it depends on $A(0)$.

Figure 3 shows G_I in Eq. (43) and G_I^{∞} in Eq. (56) at $p(0, 0, 0)$ against b induced by a source at $q(0, 0, -H/100)$ with wave number $k_0 = 2$. Because $x - \xi = 0$, Eqs. (56) and (57) are identical in this special case. Three ice sheet thicknesses are considered, i.e., $h = 0.1$, 1, and 5 m, which are within the typical range of field observations.[38] It can be seen from the figure that as b increases, G_I^{∞} becomes closer and closer to G_I, and their modulus oscillate with b and decrease slowly at the same time, as shown in Eq. (56). When the ice sheet thickness is very small, G_I becomes negligible. When h increases, the modulus of G_I becomes larger, i.e., the ice sheet has a much stronger effect or the reflected wave by the ice sheet due to $F(p, q)$ has a much larger amplitude.

C. The effectiveness of irregular frequency removal method

When Eq. (27) is discretized, a matrix equation for the potentials at panels can be obtained. Away from the irregular frequencies, the equation can be solved using standard methods and accurate results can be obtained. However, the matrix equation becomes ill-conditioned at irregular frequencies. The obtained results near the irregular frequencies vary almost vertically or they are highly oscillatory, which is not due to true physical reason but due to deficiency of the mathematical method. Therefore, following Lee, Newman, and Zhu,[34] Eq. (27) is modified into two equivalent equations, or Eqs. (28) and (29). Figures 4 and 5, respectively, depict the added mass and damping coefficient against the wavenumber k_0 computed from (27), and also that from combined (28) and (29). The two sets of results are generally in good agreement, as they should be. Near the irregular frequencies the results from the former have spikes, while those from the latter are smooth. This shows that Eqs. (28) and (29) have successfully removed irregular frequencies.

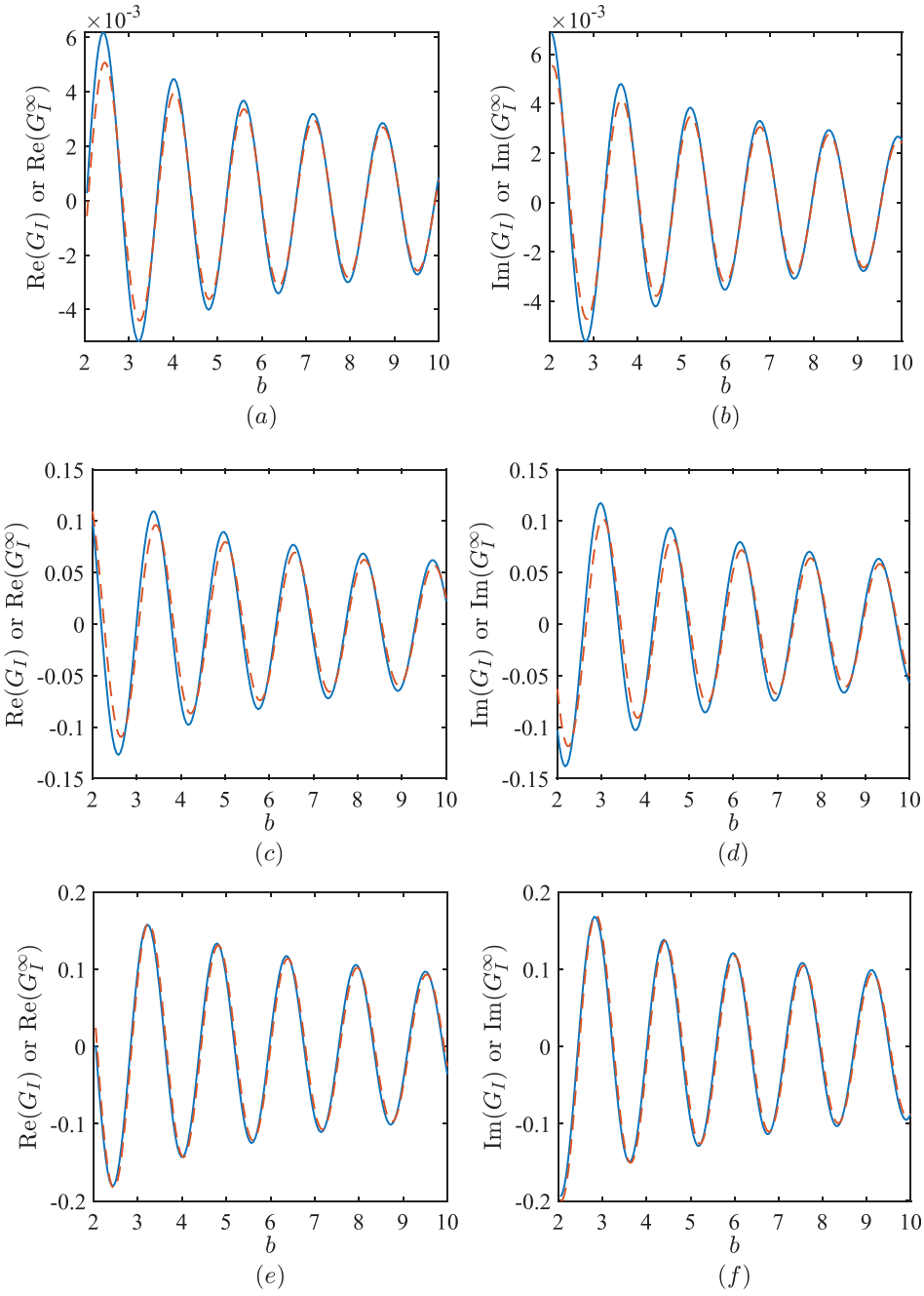

FIG. 3. G_I and G_I^∞ at $p(0,0,0)$ against b induced by a source at $q(0,0,-H/100)$ ($k_0 = 2$). (a) and (b) are for $h = 0.1$ m; (c) and (d) are for $h = 1$ m; (e) and (f) are for $h = 5$ m. Re is for real part and Im is for imaginary part. Solid lines: G_I [Eq. (43)]; dashed lines: G_I^∞ [Eq. (56)].

D. Approximate solution for a ship away from the ice edge

When the distance b between the ship and ice sheet is large, we may write $\varepsilon = (x-\xi)/(2b-y-\eta)$. When $\varepsilon \to 0$, from Eq. (54) $\alpha_0 = O(\varepsilon)$. When $A(\alpha_0)$ in Eq. (56) is replaced by $A(0)$, the ignored term is of order $O(\varepsilon)$. With this approximation, when b is large, by ignoring the $\varepsilon^{3/2}$ term in Eq. (56), the Green function in Eq. (18) may be approximated as

$$G(p,q) \approx F(p,q) + A(0)I(p,q) \ (y \le b-0), \tag{58}$$

where

$$I(p,q) = Z_0(z)Z_0(\zeta)\sqrt{\frac{2\pi}{k_0\bar{R}}}e^{-i\left(k_0\bar{R}-\frac{\pi}{4}\right)}. \tag{59}$$

Invoking Eqs. (37) and (38), we have that $A(0)$ is independent of the source and field positions, as well as the distance b. However, it is

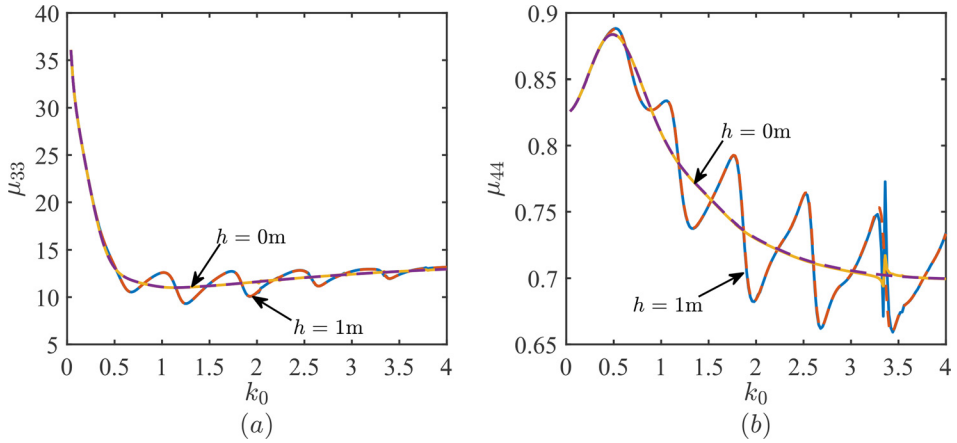

FIG. 4. Added mass in heave mode μ_{33} (a) and roll mode μ_{44} (b) against k_0 with $b = 5$. Solid lines: by Eq. (27); dashed lines: by Eqs. (28) and (29).

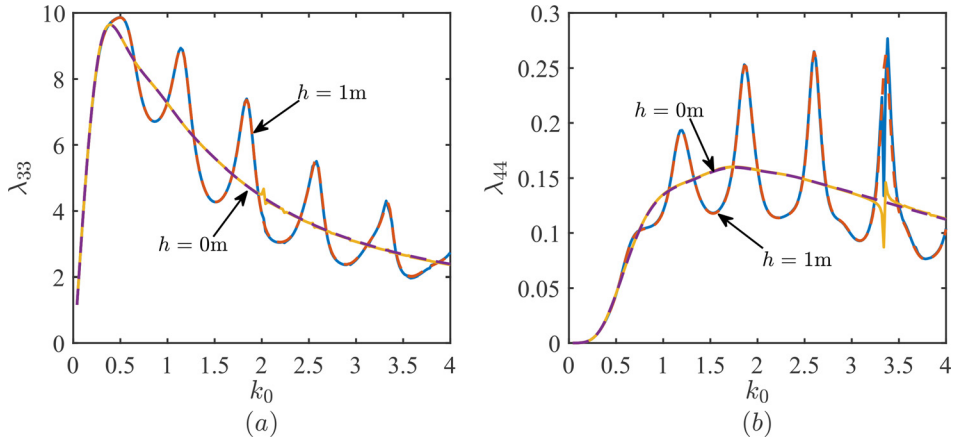

FIG. 5. Damping coefficient in heave mode λ_{33} (a) and roll mode λ_{44} (b) against k_0 with $b = 5$. See the caption of Fig. 4 for further information.

affected by the properties of the ice sheet. Nevertheless, for a given wave frequency and ice sheet, $A(0)$ only needs to be computed once, which significantly reduces the CPU requirement. Figures 6 and 7 show the diagonal terms of the added mass and damping coefficients against the distance b. The wavenumber is taken to be $k_0 = 2$. It can be seen from these two figures that as in the range of b calculated, especially at large value, the difference between the solid lines [using the Green function in Eq. (18)] and dashed lines [using the approximation in Eq. (58)] is very small. This shows that the approximate method can predict the hydrodynamic force with a high accuracy,

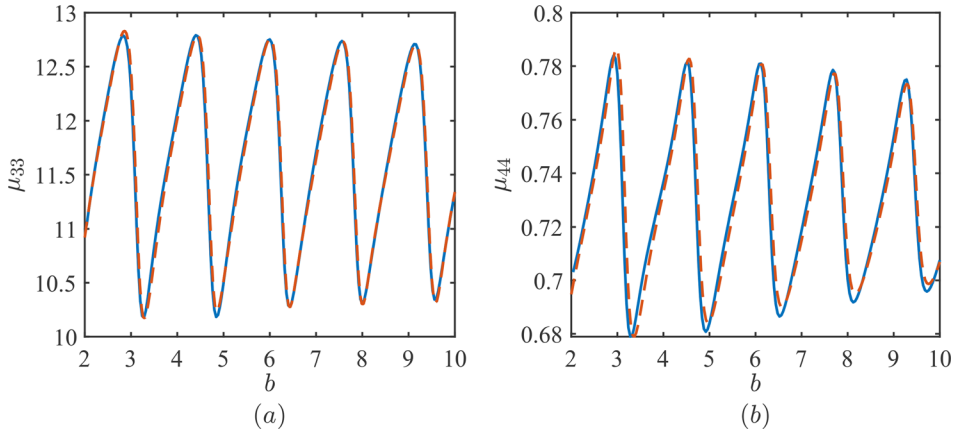

FIG. 6. Added mass in heave mode μ_{33} (a) and roll mode μ_{44} (b) against b ($h = 1$ m and $k_0 = 2$). Solid lines: by Eq. (18); dashed lines: by Eq. (58).

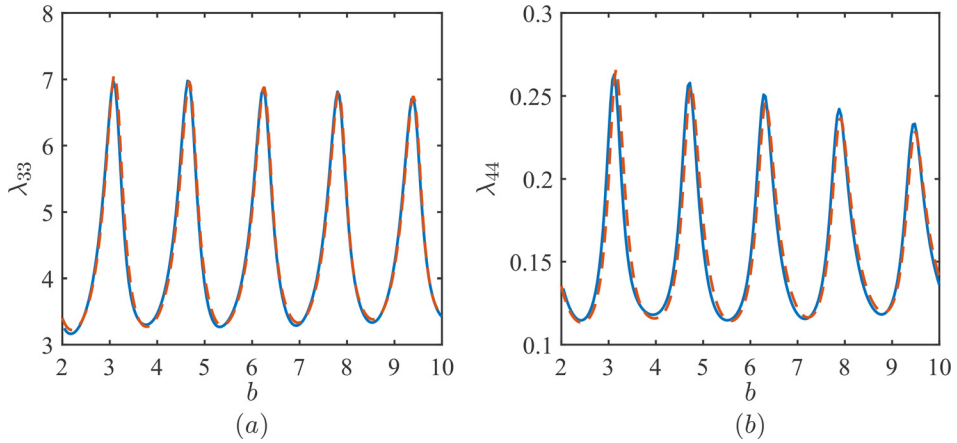

FIG. 7. Damping coefficient in heave mode λ_{33} (a) and roll mode λ_{44} (b) against b. See the caption of Fig. 6 for further information.

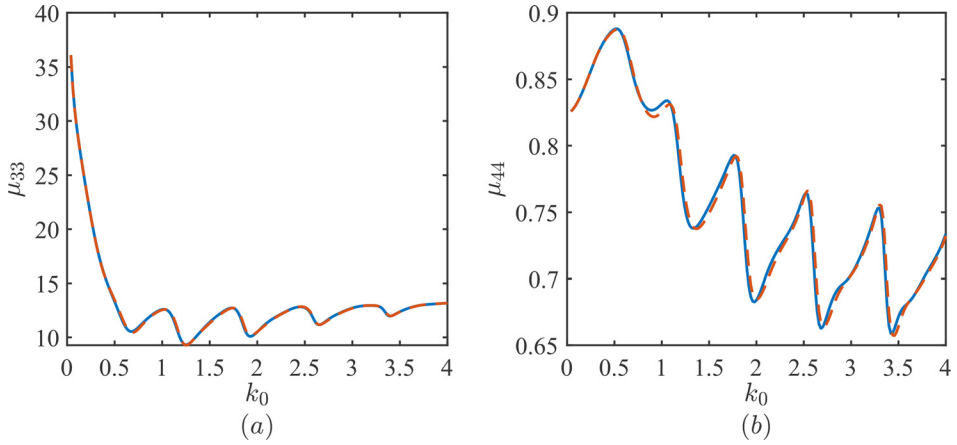

FIG. 8. Added mass in heave mode μ_{33} (a) and roll mode μ_{44} (b) against k_0 ($h = 1$ m and $b = 5$). Solid lines: by Eq. (18); dashed lines: by Eq. (58).

while it is also computationally far more efficient. At a given distance $b = 5$, the diagonal terms of the added mass and damping coefficients are provided in Figs. 8 and 9, respectively. It can be seen from the figures that the hydrodynamic force computed using Eq. (58) agrees well with that by the exact Green function (18), although the distance b is only five times of the half ship width or a third of the ship length. This is the case in the whole range of wavenumber, including very small k_0 or very long wavelength.

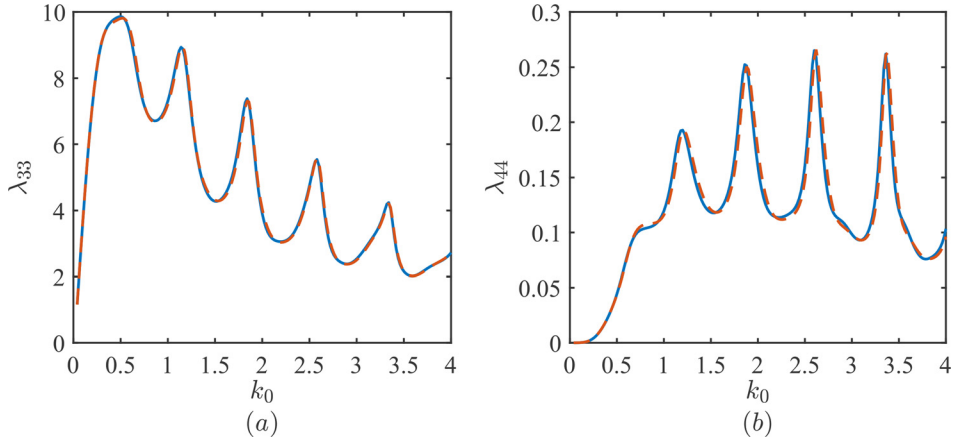

FIG. 9. Damping coefficient in heave mode λ_{33} (a) and roll mode λ_{44} (b) against k_0. See the caption of Fig. 8 for further information.

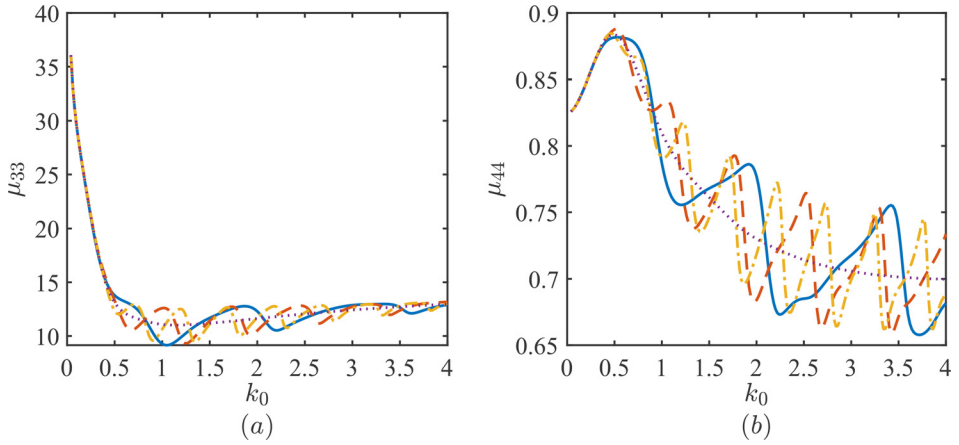

FIG. 10. Added mass in heave mode μ_{33} (a) and roll mode μ_{44} (b) at different distances from the ice edge against k_0 ($h = 1$ m and $\beta = \pi/2$). Solid lines: $b = 3$; dashed lines: $b = 5$; dash-dotted lines: $b = 7$; dotted lines: open water.

E. The effect of distance of a ship from the ice edge

In Secs. IV E–IV G, the solution procedure in Sec. III will be applied to compute the hydrodynamic coefficients and wave exciting force, while the approximate solution in Sec. IV D will be used to investigate the mechanism behind the behaviors of the results. We consider wave interactions with a ship floating on the water surface with its longitudinal direction parallel to the ice edge. Three transverse distances are considered, i.e., $b = 3, 5, 7$. The incident wave from open sea is normal to the ice edge or $\beta = \pi/2$, which also means beam sea to the ship. The ice sheet thickness is chosen to be $h = 1$ m. The diagonal terms of the added mass and damping coefficients are, respectively, shown in Figs. 10 and 11 against the wavenumber k_0, while the modulus of the wave exciting force is provided in Fig. 12. In these figures, the results for open water are also provided for comparison. In numerical calculations, the wavenumber k_0 varies from 0.04 to 4 with a step 0.02. To investigate any possible sharp variation of the results, the step can be easily reduced further.

It can be seen from Figs. 10 and 11 that the hydrodynamic coefficients will tend to those for open sea as $k_0 \to 0$, as the boundary conditions on both ice sheet and free surface will tend to be that for a rigid lid or $\partial\phi_j/\partial z = O(\omega^2)$. Also, when $\omega \to 0$ the forced oscillations of a ship will be almost like quasi-static motion, the disturbed waves will become very small, and the damping coefficient will tend to zero, as shown in Fig. 11. For the diffraction problem, it can be observed from Fig. 12 that all the wave exciting force tend to zero except those in the heave mode and pitch mode which tend to a finite value. This is because that as k_0 tends to zero or the wavelength tends to infinity, the wave dynamic effect will disappear or the diffracted velocity potentials ϕ_D^1 and ϕ_D^2 in Eq. (30) will be zero. Then, Eq. (34) becomes

$$f_{E,j} = -\mathrm{i}\omega\rho_w \int_{S_B} \phi_I n_j \mathrm{d}s = \rho_w g \int_{S_B} n_j \mathrm{d}s. \tag{60}$$

For translational mode, Eq. (60) indicates that only $f_{E,3}$ is nonzero; while for rotational mode, only $f_{E,5}$ will be nonzero since the ship is symmetric about its longitudinal plane passing the rotational center and asymmetric about the corresponding transverse plane.

As the wavenumber k_0 increases, the hydrodynamic force for different b starts to depart from each other and all oscillate around that for open sea, which changes smoothly against k_0. As the disturbed free surface wave generated by the ship encounters the ice sheet, the wave will be significantly altered. Part of wave will be reflected. Upon encountering the ship, the reflected wave may be at its peak or through depending on the ratio of the wavelength to b, leading to the oscillatory features of the hydrodynamic force. This may be further explained

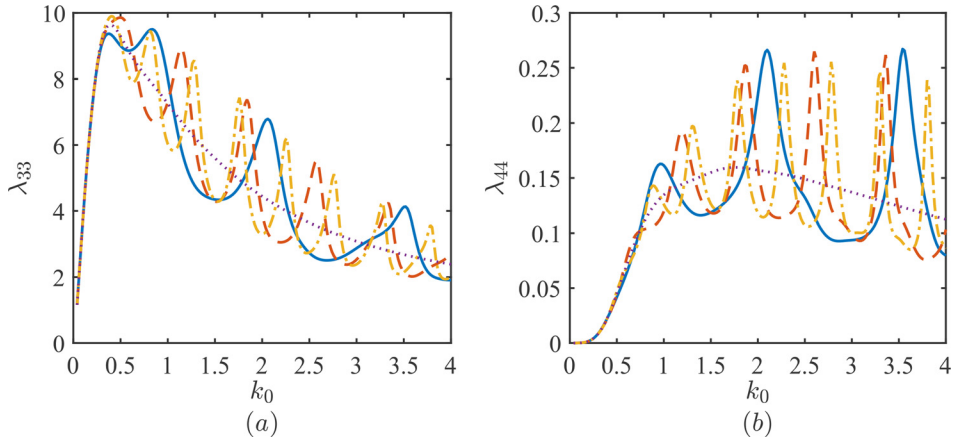

FIG. 11. Damping coefficient in heave mode λ_{33} (a) and roll mode λ_{44} (b) at different distances from the ice edge against k_0. See the caption of Fig. 10 for further information.

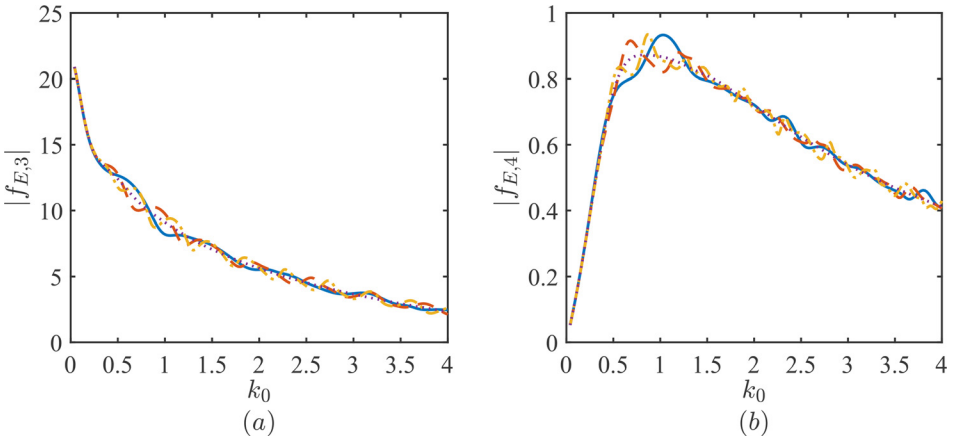

FIG. 12. Wave exciting force in heave mode $f_{E,3}$ (a) and roll mode $f_{E,4}$ (b) at different distances from the ice edge against k_0. See the caption of Fig. 10 for further information.

through the asymptotic form of the Green function. According to Eq. (57), there is an oscillatory term in form of $\exp(-2ik_0b)$. For a fixed b, the period of oscillation with k_0 will be π/b. In terms of k_0, this becomes π/b, as can be observed from Figs. 10–12. For a fixed k_0, the period of oscillation with b will be π/k_0, and in terms of b this becomes π/k_0, as can be seen in Figs. 6 and 7 of Sec. IV D for the added mass and damping coefficient, respectively. As $k_0 = 2$, the period is equal to $\pi/2$. The results in Figs. 5 and 6 also decay slowly with b, which is consistent with Eq. (57). From Eq. (57), the effect of the ice sheet at a given k_0 will disappear as $b \to \infty$. This is different from the 2D problem, where the effect of ice sheet on the hydrodynamic force will always be there even if $b \to \infty$ (e.g., Li, Shi and Wu[20]).

F. The effect of ice sheet thickness

We then investigate the effect of ice sheet thickness on the hydrodynamic force. Three different ice sheet thicknesses are considered, i.e., $h = 0.1$, 1, 5 m, together with the case for open water or $h = 0$. The incident wave angle is taken to be $\beta = \pi/2$, and the distance between ship and ice edge is chosen as $b = 5$. Figures 13 and 14 show the diagonal terms of the added mass and damping coefficients against the wavenumber k_0, and Fig. 15 demonstrates the modulus of the wave exciting force. The range and step of abscissa are the same as those in Sec. IV E.

When $k_0 \to 0$, the hydrodynamic force for ice sheet with different thickness all tends to the same value as the boundary condition on the upper surface tends to be the same. As the wavenumber k_0 increases, the hydrodynamic force with different h starts to depart from each other. When the ice sheet thickness tends to zero, the hydrodynamic force will tend to that for open water, e.g., from $h = 5$ m to $h = 0.1$ m shown in the figures. In fact, if we set $h = 0$ directly in Eq. (38), it can be shown that $b_m = e^{-i\beta_m(b-\eta)}Z_m(\zeta)/(i\beta_m P_m)$, and then $a_m = 0$ in Eq. (37), i.e., the Green function in Eq. (18) will become that for open water.

When h increases, the hydrodynamic force oscillates around that for open water with a much larger amplitude. As discussed by Li, Shi and Wu[20] for a 2D wave/body/ice sheet interaction problem, the oscillatory behavior strongly depends on the reflection coefficient by the ice sheet, and a larger $|R^o|$ may lead to much larger peaks and smaller troughs. We may use the 2D results as an indication here. In Fig. 16, the variations of κ_0 and $|R^o|$ of normal incident against the wavenumber k_0 at different ice thicknesses are provided. It can be observed that with the increase in ice thickness, the flexural-gravity wavenumber

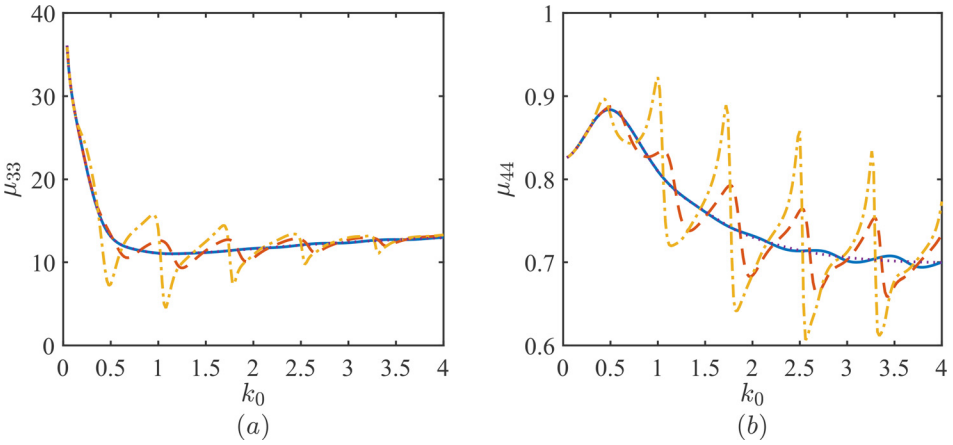

FIG. 13. Added mass in heave mode μ_{33} (a) and roll mode μ_{44} (b) at different ice sheet thicknesses against k_0 ($b = 5$ and $\beta = \pi/2$). Solid lines: $h = 0.1$ m; dashed lines: $h = 1.0$ m; dash-dotted lines: $h = 5.0$ m; dotted lines: open water.

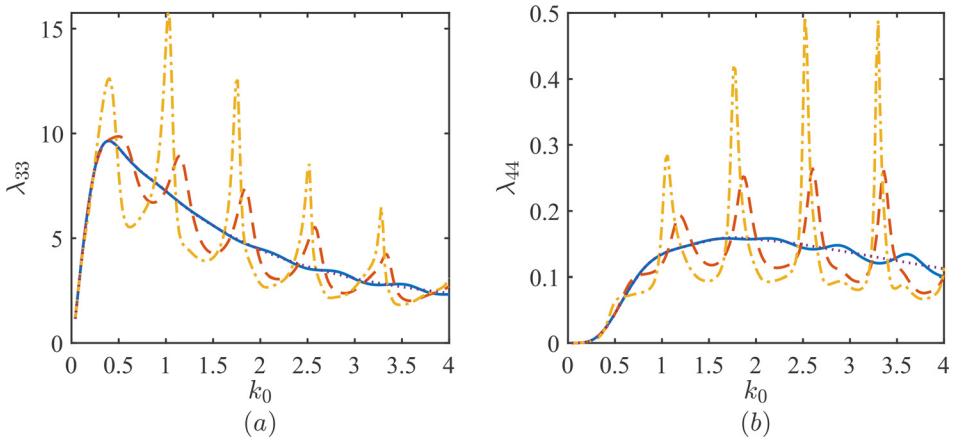

FIG. 14. Damping coefficient in heave mode λ_{33} (a) and roll mode λ_{44} (b) at different ice sheet thicknesses against k_0. See the caption of Fig. 13 for further information.

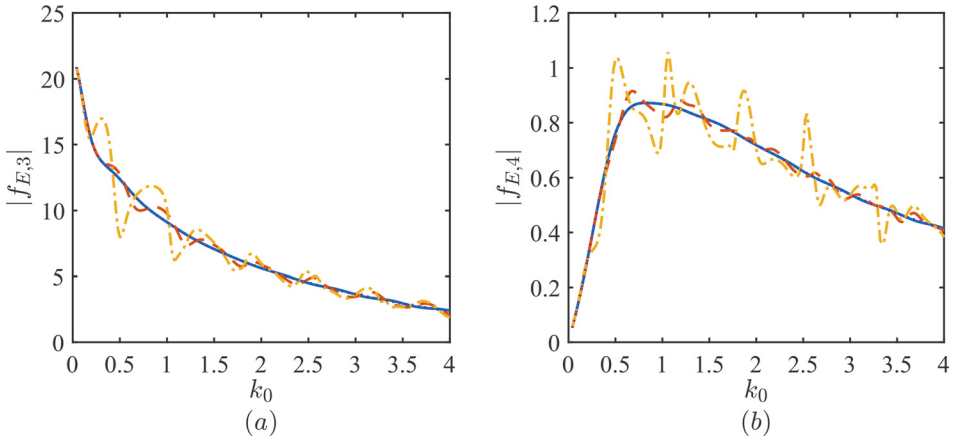

FIG. 15. Wave exciting force in heave mode $f_{E,3}$ (a) and roll mode $f_{E,4}$ (b) at different ice sheet thicknesses against k_0. See the caption of Fig. 13 for further information.

decreases, while the reflection coefficient increases. This means that the interaction between ice sheet and a body nearby becomes much stronger. In 2D problems, the reflected wave by an ice sheet due to a line source is a plane wave, and its amplitude does not decrease during its propagation. However, in 3D problems, Eq. (59) indicates that the reflection wave is a ring wave with its center at the mirror image position of the source point with respect to the ice edge. $A(0)$ in Eq. (58) can be used as a measurement of its amplitude, which further

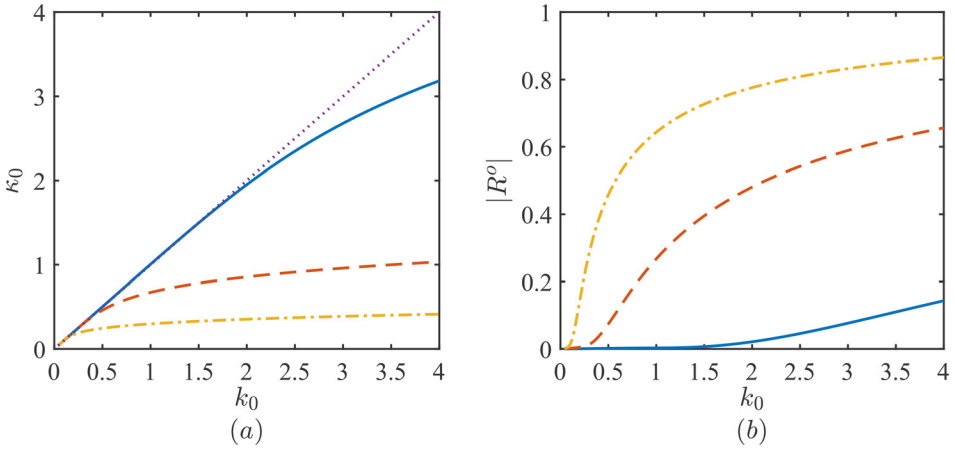

FIG. 16. Flexural-gravity wave number (a) and 2D reflection coefficient (b) against k_0 ($\beta = \pi/2$). Solid lines: $h = 0.1$ m; dashed lines: $h = 1.0$ m; dash-dotted lines: $h = 5.0$ m; dotted lines in (a): $h = 0$ m.

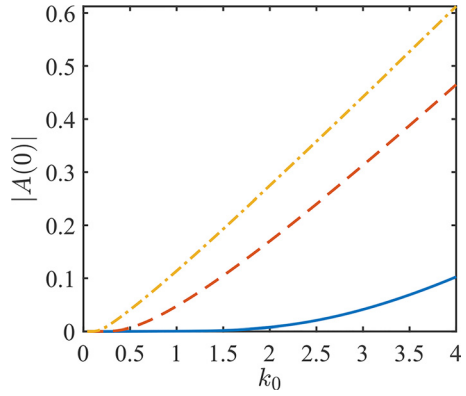

FIG. 17. The modulus of $A(0)$ in Eq. (58) against k_0. Solid lines: $h = 0.1$ m; dashed lines: $h = 1.0$ m; dash-dotted lines: $h = 5.0$ m.

determines the oscillatory amplitude of the hydrodynamic force. Therefore, in Fig. 17 we plot the modulus of $A(0)$ against k_0 at different ice sheet thickness. It can be seen from Fig. 17 that $|A(0)|$ increases with h, leading to a much larger oscillatory amplitude of the hydrodynamic force. In fact, the left-hand sides of Eqs. (A6) and (A7) with $k_x = 0$ are the same as those of Eqs. (21) and (22) at $\alpha = 0$. Their solutions should be similar. Noticing for $R^o = \bar{a}_0/A$ where A is given below Eq. (32), and $A(0)$ obtained from Eqs. (37) and (38), the variations of $|R^o|$ and $|A(0)|$ with respect to h are expected to be similar.

G. The effect of incident wave angle on the wave exciting force

Finally, we consider the effect of incident wave angle on the wave exciting force. Four different incident wave angles are considered, i.e., $\beta = \pi/2, \pi/3, \pi/6$ and $\pi/18$. The first one indicates that the incident wave propagates normally to the ice sheet, while the last one corresponds to that nearly parallel to the ice sheet. The ice sheet thickness is taken to be $h = 1$m, and the distance between ship and ice edge is chosen as $b = 5$. Figure 18 shows the wave exiting force $f_{E,j}$ against the wavenumber k_0, while Figs. 19 and 20 depict the corresponding Froude–Krylov force $f^I_{E,j}$ due to $\varphi = \phi_I + \phi^{(1)}_D$ and the wave diffraction force $f^D_{E,j}$ due to $\phi^{(2)}_D$, or

$$f^I_{E,j} = -\mathrm{i}\omega\rho_w \int_{S_B} \varphi n_j \mathrm{d}s, \tag{61}$$

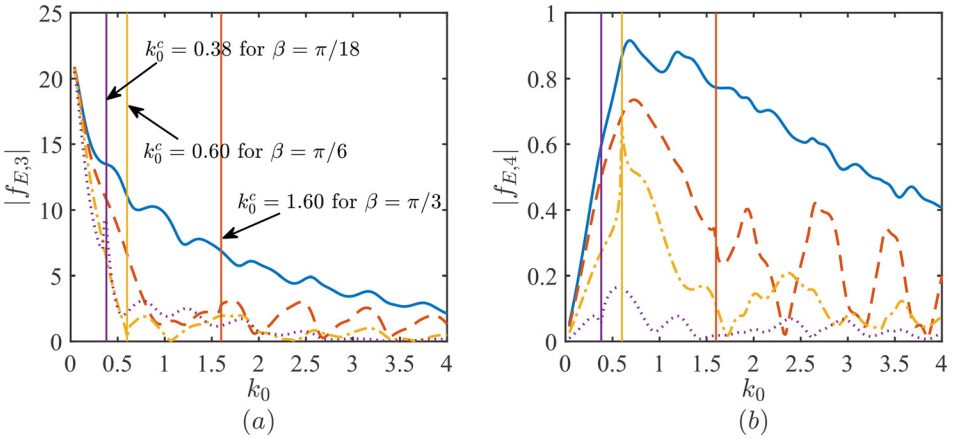

FIG. 18. Wave exciting force in heave mode $f_{E,3}$ (a) and roll mode $f_{E,4}$ (b) at different incident wave angles against k_0 ($b = 5$ and $h = 1.0$ m). Solid lines: $\beta = \pi/2$; dashed lines: $\beta = \pi/3$; dash-dotted lines: $\beta = \pi/6$; dotted lines: $\beta = \pi/18$.

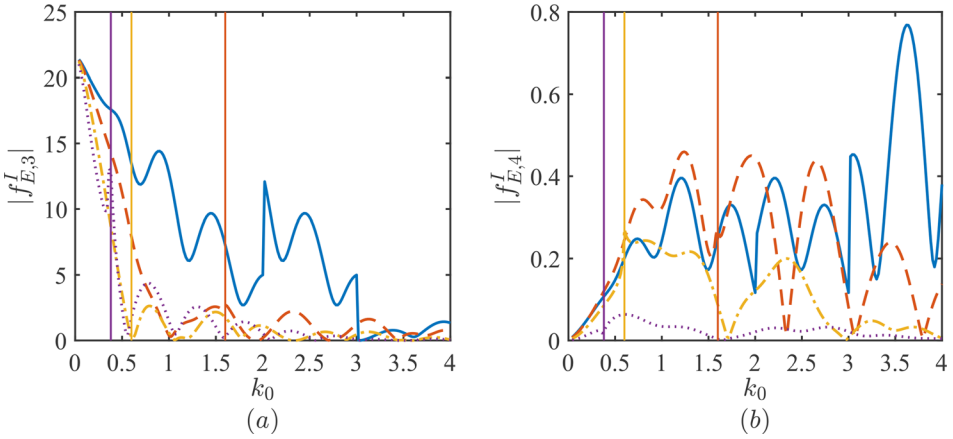

FIG. 19. Froude–Krylov force in heave mode $f^I_{E,3}$ (a) and roll mode $f^I_{E,4}$ (b) due to φ at different incident wave angles against k_0. See the caption of Fig. 18 for further information.

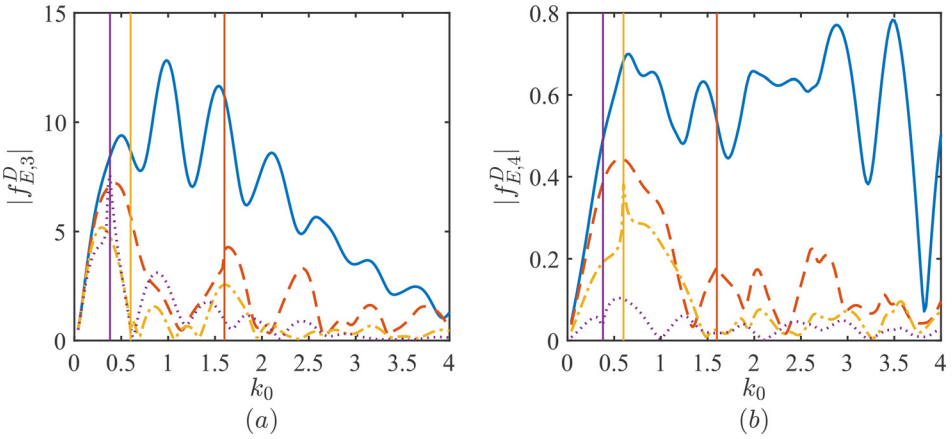

FIG. 20. Wave diffraction force in heave mode $f^D_{E,3}$ (a) and roll mode $f^D_{E,4}$ (b) due to $\phi^{(2)}_D$ at different incident wave angles against k_0. See the caption of Fig. 18 for further information.

$$f^D_{E,j} = -\mathrm{i}\omega\rho_w \int_{S_B} \phi^{(2)}_D n_j \mathrm{d}s. \tag{62}$$

The range and step of abscissa are the same as those in Sec. IV E.

It can be seen from the figures that as k_0 is small the wave exciting force is not affected by the incident wave angle very much. This is because that the dynamic effect of fluid motion is small in this case, and the effect of β disappears. As k_0 increases, $f_{E,j}$ for different β departs from each other evidently. Generally, the magnitude of wave exciting force has more local peaks and troughs against k_0 than the radiation force shown through μ_{jj} and λ_{jj} in Figs. 13 and 14. This is because the velocity potential φ, which is a combination of ϕ_I and $\phi^{(1)}_D$ by the ice sheet due to ϕ_I, also oscillates with k_0, leading to the local peaks and troughs of Froude–Krylov force $f^I_{E,j}$, as shown in Fig. 19. When we impose the boundary condition in the boundary integral equations (28) and (29), or $\partial\phi^{(2)}_D/\partial n = -\partial\varphi/\partial n$, both the Green function G and φ will contribute to the oscillations of $\phi^{(2)}_D$. While for the wave radiation problem, only G will have contributions to the local oscillations as $\partial\phi_j/\partial n = n_j$ is imposed on S_B.

When β varies from $\pi/18$ to $\pi/2$, the wave exciting forces in sway, heave and roll tend to increase overall. For the oblique incident wave case, Fox and Squire[3] have shown that a critical angle exists, smaller than which the refection coefficient $|R^o| = 1$. Equivalently, it means that at a given β, κ_0/k_0 has a critical value. Below that, there is no transmission into ice sheet and there will be full refection, and above that transmission can happen. At $\beta = \pi/3$, $\pi/6$ and $\pi/18$, the critical value of κ_0/k_0 are at 0.50, 0.87 and 0.98, respectively, and the corresponding values of wave number k^c_0 are marked in Figs. 18–20. As shown in Fig. 16(a), κ_0/k_0 decreases as k_0 increases except at small k_0. Therefore, on the right hand side of the critical value marked in the figures, there will be no transmission. Figure 21 shows when k_0 approaches the critical number from the left, $|R^o|$ from different β all increase to 1 very fast, and beyond the critical number $|R^o| = 1$, indicating a full reflection. Correspondingly, there is a rapid variation of the wave exciting force in Figs. 18–20 when k_0 increases to the critical value, which is evident when the magnitude of the force is big in the figure.

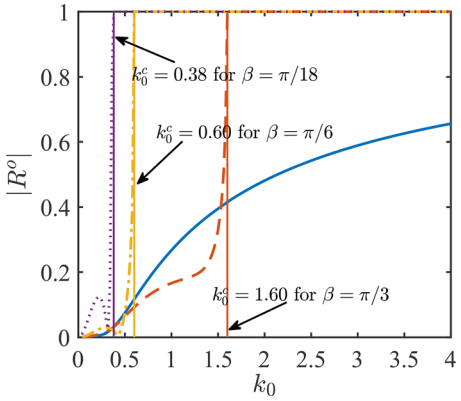

FIG. 21. Reflection coefficient against k_0 at different incident wave angles ($h = 1.0$ m). Solid lines: $\beta = \pi/2$; dashed lines: $\beta = \pi/3$; dash-dotted lines: $\beta = \pi/6$; dotted lines in (a): $\beta = \pi/18$.

V. CONCLUSIONS

The problem of wave interactions with a ship floating on the water surface near a semi-infinite ice sheet has been solved based on the linearized velocity potential theory for fluid motion and thin elastic plate model for the ice sheet deflection. The Green function, satisfying all the boundary conditions including those on the ice sheet and free surface, apart from that on the ship surface, is derived. Through the Green function, the differential equation for the disturbed velocity potential is transformed into a boundary integral equation over the ship surface only, and the effect of irregular wave frequencies is removed through modification of the integral equation which is solved based on the boundary element method.

An asymptotic formula of the Green function is derived when the transverse distance b between the source and ice sheet is large. This reveals that the effect of an ice sheet is equivalent to place another source at the mirror image location with respect to the ice edge. However, the strength of the source at the mirror image is different from the original one, and it depends on the physical properties of the ice sheet. The result is, therefore, different from that of a vertical wall. As the ice sheet thickness increases, the strength of the mirror source will increase. Through the asymptotic formula of the Green function, an approximate and efficient solution procedure is developed. Although it is based on the assumption that a ship is far away from

the ice sheet, it is found that the approximate method can predict the hydrodynamic force with a high accuracy in the whole range of wavenumbers calculated, including very large wavelength even when the ship is close to the ice edge. At the same time, the method is computationally far more efficient.

Different from a ship floating in open water, the existence of the ice sheet will lead to an oscillatory behavior of the hydrodynamic force. Specifically, the asymptotic solution procedure shows that at a fixed b, the period of oscillation of the hydrodynamic force with wavenumber k_0 will be π/b, while in terms of b it will be π/k_0. This indicates that a larger b will lead to a more oscillatory hydrodynamic force against k_0. As $b \to \infty$, the effect of the ice sheet at a given k_0 will disappear, which is different from that in the two-dimensional problem. More wave energy will be reflected back to the ship by the ice sheet when it becomes thicker, leading to the hydrodynamic force having a much larger oscillatory amplitude. The wave exciting force has more peaks and troughs than the added mass and damping coefficient due to the interactions between incident wave and the ice sheet. For oblique incident wave with angle β, the wave exciting force will have a rapid variation around the critical wavenumber at which $\cos\beta = \kappa_0/k_0$ with κ_0 being the flexural-gravity wavenumber.

ACKNOWLEDGMENTS

This work is supported by the National Natural Science Foundation of China (Grant Nos. 52071162, 52025112, 51709131, and 51879123). This work is also supported by Lloyd's Register Foundation, to which the authors are most grateful. Lloyd's Register Foundation helps to protect life and property by supporting engineering-related education, public engagement, and the application of research.

AUTHOR DECLARATIONS

Conflict of Interest

The authors report no conflict of interest.

DATA AVAILABILITY

The data that support the findings of this study are available from the corresponding author upon reasonable request.

APPENDIX: DIFFRACTED VELOCITY POTENTIAL BY THE ICE SHEET TO THE INCIDENT WAVE

Substituting Eq. (33) or $\varphi = \bar{\varphi}(y,z)e^{-ik_x x}$ into the governing Eq. (2), we have that $\bar{\varphi}$ should satisfy the Helmholtz equation throughout the fluid, or

$$-k_x^2\bar{\varphi} + \frac{\partial^2\bar{\varphi}}{\partial y^2} + \frac{\partial^2\bar{\varphi}}{\partial z^2} = 0, \tag{A1}$$

and the same boundary conditions as those for $\tilde{G}$, but with α being replaced by k_x. In the free surface part of fluid, we may write $\bar{\varphi}$ as

$$\bar{\varphi} = \bar{\varphi}_f = \varphi_I(y,z) + \sum_{m=0}^{\infty} \bar{a}_m \bar{\psi}_m^f \quad (y \le b-0), \tag{A2}$$

with

$$\bar{\psi}_m^f = e^{-i\bar{\beta}_m(b-y)} Z_m(z), \tag{A3}$$

where $\bar{\beta}_m^2 = k_m^2 - k_x^2$, and $\mathrm{Im}(\bar{\beta}_m) \le 0$ when it is a complex number and $\bar{\beta}_m > 0$ when it is a purely real number. In the ice-covered part of fluid, we may write $\bar{\varphi}$ as

$$\bar{\varphi} = \bar{\varphi}_i = \sum_{m=-2}^{\infty} \bar{b}_m \bar{\psi}_m^i \quad (y \ge b+0), \tag{A4}$$

where

$$\bar{\psi}_m^i = e^{-i\bar{\gamma}_m(y-b)} Q_m(z). \tag{A5}$$

Here, $\bar{\gamma}_m^2 = \kappa_m^2 - k_x^2$, and $\mathrm{Im}(\bar{\gamma}_m) \le 0$ when it is a complex number, and $\bar{\gamma}_m > 0$ when it is a purely real number based on the requirement of the radiation condition. Then, similar to Eqs. (21) and (22), we can obtain

$$\bar{\gamma}_m \sum_{\tilde{m}=0}^{\infty} \bar{a}_{\tilde{m}} V_{m,\tilde{m}} - \bar{b}_m \bar{\gamma}_m U_m - \frac{LT_m}{\rho_w \omega^2} \sum_{\tilde{m}=-2}^{\infty} \bar{b}_{\tilde{m}} T_{\tilde{m}} \{\nu k_x^2 (\bar{\gamma}_{\tilde{m}} + \bar{\gamma}_m) - 2k_x^2 \bar{\gamma}_m + \bar{\gamma}_m^2 (\bar{\gamma}_{\tilde{m}} - \bar{\gamma}_m) - \bar{\gamma}_{\tilde{m}} (\kappa_m^2 + \kappa_{\tilde{m}}^2)\} = -\bar{\gamma}_m A e^{-ik_y b} V_{m,0}, \tag{A6}$$

$$-\bar{\beta}_m P_m \bar{a}_m - \sum_{\tilde{m}=-2}^{\infty} \bar{b}_{\tilde{m}} \bar{\gamma}_{\tilde{m}} V_{\tilde{m},m} = -k_y A e^{-ik_y b} \delta_{m0} P_m. \tag{A7}$$

The infinite summations in Eqs. (A2) and (A4) can be truncated at a finite number, and the matrix equation can be solved, the coefficients $\bar{a}_m$ and $\bar{b}_m$, and subsequently the potential φ can be obtained.

REFERENCES

[1] V. A. Squire, "Ocean wave interactions with sea ice: A reappraisal," Annu. Rev. Fluid Mech. **52**, 37 (2020).
[2] C. Fox and V. A. Squire, "Reflection and transmission characteristics at the edge of shore fast sea ice," J. Geophys. Res.: Oceans **95**, 11629–11639, https://doi.org/10.1029/JC095iC07p11629 (1990).
[3] C. Fox and V. A. Squire, "On the oblique reflexion and transmission of ocean waves at shore fast sea ice," Philos. Trans. R. Soc. **A 347**, 185 (1994).
[4] T. Sahoo, T. L. Yip, and A. T. Chwang, "Scattering of surface waves by a semi-infinite floating elastic plate," Phys. Fluids **13**, 3215 (2001).
[5] N. J. Balmforth and R. V. Craster, "Ocean waves and ice sheets," J. Fluid Mech. **395**, 89 (1999).
[6] C. Fox and V. A. Squire, "Coupling between the ocean and an ice shelf," Ann. Glaciol. **15**, 101 (1991).
[7] L. A. Tkacheva, "The diffraction of surface waves by a floating elastic plate at oblique incidence," J. Appl. Math. Mech. **68**, 425 (2004).
[8] A. Chakrabarti, "On the solution of the problem of scattering of surface-water waves by the edge of an ice cover," Proc. R. Soc. London, Ser. A **456**, 1087 (2000).
[9] C. M. Linton and H. Chung, "Reflection and transmission at the ocean/sea-ice boundary," Wave Motion **38**, 43 (2003).
[10] A. Dolatshah, F. Nelli, L. G. Bennetts, A. Alberello, M. H. Meylan, J. P. Monty, and A. Toffoli, "Letter: Hydroelastic interactions between water waves and floating freshwater ice," Phys. Fluids **30**, 091702 (2018).
[11] Y. Y. Shi, Z. F. Li, and G. X. Wu, "Interaction of wave with multiple wide polynyas," Phys. Fluids **31**, 067111 (2019).
[12] H. Liang and X. B. Chen, "A new multi-domain method based on an analytical control surface for linear and second-order mean drift wave loads on floating bodies," J. Comput. Phys. **347**, 506 (2017).
[13] Y. Y. Shi, Z. F. Li, and G. X. Wu, "Motion of a floating body in a harbour by domain decomposition method," Appl. Ocean Res. **78**, 223 (2018).

[14]J. N. Newman, "Trapped-wave modes of bodies in channels," J. Fluid Mech. **812**, 178 (2017).
[15]I. V. Sturova, "Wave generation by an oscillating submerged cylinder in the presence of a floating semi-infinite elastic plate," Fluid Dyn. **49**, 504 (2014).
[16]I. V. Sturova, "Radiation of waves by a cylinder submerged in water with ice floe or polynya," J. Fluid Mech. **784**, 373 (2015).
[17]L. A. Tkacheva, "Oscillations of a cylindrical body submerged in a fluid with ice cover," J. Appl. Mech. Tech. Phys. **56**, 1084 (2015).
[18]K. Ren, G. X. Wu, and G. A. Thomas, "Wave excited motion of a body floating on water confined between two semi-infinite ice sheets," Phys. Fluids **28**, 127101 (2016).
[19]Z. F. Li, Y. Y. Shi, and G. X. Wu, "Interaction of waves with a body floating on polynya between two semi-infinite ice sheets," J. Fluids Struct. **78**, 86 (2018).
[20]Z. F. Li, Y. Y. Shi, and G. X. Wu, "Interaction of wave with a body floating on a wide polynya," Phys. Fluids **29**, 097104 (2017).
[21]F. Ursell, "On the heaving motion of a circular cylinder on the surface of a fluid," Q. J. Mech. Appl. Math. **2**, 218 (1949).
[22]L. A. Tkacheva, "Oscillations of a cylinder beneath an ice cover in the neighborhood of a vertical wall," Fluid Dyn. **55**, 300 (2020).
[23]Z. F. Li, G. X. Wu, and C. Y. Ji, "Wave radiation and diffraction by a circular cylinder submerged below an ice sheet with a crack," J. Fluid Mech. **845**, 682 (2018).
[24]Z. F. Li, Y. Y. Shi, and G. X. Wu, "Large amplitude motions of a submerged circular cylinder in water with an ice cover," Eur. J. Mech. B-Fluids **65**, 141 (2017).
[25]P. Brocklehurst, A. A. Korobkin, and E. I. Părău, "Hydroelastic wave diffraction by a vertical cylinder," Philos. Trans. R. Soc. **369**, 2832 (2011).
[26]A. A. Korobkin, S. Malenica, and T. Khabakhpasheva, "Interaction of flexural-gravity waves in ice cover with vertical walls," Philos. Trans. R. Soc. **376**, 20170347 (2018).
[27]K. Ren, G. X. Wu, and C. Y. Ji, "Diffraction of hydroelastic waves by multiple vertical circular cylinders," J. Eng. Math. **113**, 45 (2018).
[28]K. Ren, G. X. Wu, and C. Y. Ji, "Wave diffraction and radiation by a vertical circular cylinder standing in a three-dimensional polynya," J. Fluids Struct. **82**, 287 (2018).
[29]Z. F. Li, Y. Y. Shi, and G. X. Wu, "A hybrid method for linearized wave radiation and diffraction problem by a three dimensional floating structure in a polynya," J. Comput. Phys. **412**, 109445 (2020).
[30]Z. F. Li, Y. Y. Shi, and G. X. Wu, "Interaction of ocean wave with a harbor covered by an ice sheet," Phys. Fluids **33**, 057109 (2021).
[31]Z. F. Li, G. X. Wu, and K. Ren, "Interactions of waves with a body floating in an open water channel confined by two semi-infinite ice sheets," J. Fluid Mech. **917**, A19 (2021).
[32]S. P. Timoshenko and K. S. Woinowsky, *Theory of Plates and Shells* (McGraw-Hill, Singapore, 1959).
[33]J. V. Wehausen and E. V. Laitone, *Surface Waves* (Springer Verlag, Berlin, 1960).
[34]C. H. Lee, J. N. Newman, and X. Zhu, "An extended boundary integral equation method for the removal of irregular frequency effects," Int. J. Numer. Methods Fluids **23**, 637 (1996).
[35]V. A. Squire, J. P. Dugan, P. Wadhams, P. J. Rottier, and A. K. Liu, "Of ocean waves and sea ice," Annu. Rev. Fluid Mech. **27**, 115 (1995).
[36]R. Porter, "Trapping of waves by thin floating ice floes," Q. J. Mech. Appl. Math. **71**, 463 (2018).
[37]M. Abramowitz and I. A. Stegun, *Handbook of Mathematical Functions* (Dover Press, New York, 1965).
[38]P. Wadhams, "Arctic sea ice extent and thickness," Philos. Trans. R. Soc. **A 352**, 301 (1995).